Discovering the antibacterial and antiviral properties of Flexible Solid-State Carbon Cloth Supercapacitors by Sara Beikzadeh and Prof. Jadranka Travas-Sejdic at the University of Auckland.

From energy storage to pathogen eradication: unveiling the antibacterial and antiviral capacities of flexible solid-state carbon cloth supercapacitors

Exploiting its stored electrical charge, the supercapacitor effectively disinfects bacteria and neutralizes viruses upon surface contact, achieving remarkable reductions of 6-log CFU for Escherichia coli and 5-log PFU for HSV-1 herpes virus.

As featured in:
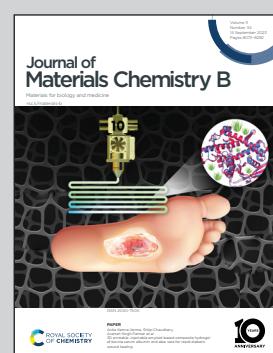
ROYAL SOCIETY OF CHEMISTRY

rsc.li/materials-b

Registered charity number: 207890

PAPER

From energy storage to pathogen eradication: unveiling the antibacterial and antiviral capacities of flexible solid-state carbon cloth supercapacitors†

Sara Beikzadeh,[ab] Alireza Akbarinejad, [ID][a] John Taylor,[c] Janesha Perera,[d] Jacqueline Ross, [ID][e] Simon Swift, [ID][d] Paul A. Kilmartin[a] and Jadranka Travas-Sejdic [ID] *[ab]

With the emergence of deadly viral and bacterial infections, preventing the spread of microorganisms on surfaces has gained ever-increasing importance. This study investigates the potential of solid-state supercapacitors as antibacterial and antiviral devices. We developed a low-cost and flexible carbon cloth supercapacitor (CCSC) with highly efficient antibacterial and antiviral surface properties. The CCSC comprised two parallel layers of carbon cloth (CC) electrodes assembled in a symmetric, electrical double-layer supercapacitor structure that can be charged at low potentials between 1 to 2 V. The optimized CCSC exhibited a capacitance of 4.15 ± 0.3 mF cm^{-2} at a scan rate of 100 mV s^{-1}, high-rate capability (83% retention of capacitance at 100 mV s^{-1} compared to its value at 5 mV s^{-1}), and excellent electrochemical stability (97% retention of the initial capacitance after 1000 cycles). Moreover, the CCSC demonstrated outstanding flexibility and retained its full capacitance even when bent at high angles, making it suitable for wearable or flexible devices. Using its stored electrical charge, the charged CCSC disinfects bacteria effectively and neutralizes viruses upon surface contact with the positive and negative electrodes. The charged CCSC device yielded a 6-log CFU reduction of *Escherichia coli* bacterial inocula and a 5-log PFU reduction of HSV-1 herpes virus. Antibacterial and antiviral carbon cloth supercapacitors represent a promising platform technology for various applications, including electronic textiles and electronic skins, health monitoring or motion sensors, wound dressings, personal protective equipment (*e.g.*, masks) and air filtration systems.

Introduction

Infectious viruses and bacteria threaten human health globally by causing acute and chronic infectious diseases.[1,2] The ongoing worldwide COVID pandemic has increased the demand for materials with active antibacterial and antiviral properties for various applications.[2–4] Therefore, developing a new generation of antibacterial and antiviral platforms with a wide range of activity and sustained effectiveness has gained extensive interest.[5,6]

Nanocarbon materials, such as single-walled and multi-walled carbon nanotubes (CNTs), fullerenes and graphene materials, have demonstrated antibacterial activities and gained interest as affordable and low-toxicity materials.[4,7–12] However, their application as biomedical agents is in its infancy compared to other antimicrobial nano-sized materials, such as silver, zinc and copper nanoparticles.[9,13–16] The antibacterial effect of these nanocarbon materials depends on their physicochemical and structural properties, including diameter, sharpness of the edges, surface functionality and electronic structure.[7–10,17] Several antibacterial mechanisms have been suggested for nanocarbon materials, including membrane puncturing and destabilization, oxidative stress and wrapping.[9,10] On the other hand, large-size carbon materials, such as carbon fibers, are cheaper, easier to manufacture and more suitable for wearable or flexible devices, however, they do not have inherent antibacterial properties.[8,18] It has been shown that the electron

[a] *Centre for Innovative Materials for Health, School of Chemical Sciences, The University of Auckland, 23 Symonds Street, Auckland, 1023, New Zealand. E-mail: j.travas-sejdic@auckland.ac.nz*

[b] *MacDiarmid Institute for Advanced Materials and Nanotechnology, Kelburn Parade, Wellington, 6140, New Zealand*

[c] *School of Biological Sciences, The University of Auckland, Auckland, New Zealand*

[d] *Department of Molecular Medicine and Pathology, Faculty of Medical and Health Sciences, The University of Auckland, Private Bag 92019, Auckland 1042, New Zealand*

[e] *Department of Anatomy and Medical Imaging, The University of Auckland, Private Bag, Auckland 92019, New Zealand*

transfer between these conductive carbon materials and bacteria could be conveniently used as an effective strategy to disrupt the bacterial respiration system and cell membrane.[19–22]

Several research studies have reported that a weak, low-voltage electric field can inactivate bacteria and destabilize viruses through different mechanisms, including electroporation and production of reactive oxygen species (ROS).[1,2,23–25] Some of these studies have shown that positively and negatively charged surfaces and particles can damage bacterial death by interacting with the cell walls and destroying the cytoplasmic membrane leading to the leakage of intracellular components.[12,22,26–29] It has been reported that nanomaterial surface modification based on charge (polarity and magnitude) shows a virucidal effect by disturbing the surface potential of viral particles and distorting the viral capsid *via* van der Waals and electrostatic interactions.[3,30,31] Applying an external low-voltage potential to different materials such as laser-induced graphene (LIG),[23,32,33] sulfur-doped LIG electrodes,[34] graphene-coated non-woven air filters,[35] Cu foam electrodes[36] and Co_3O_4 nanowires[37] have been reported to kill bacteria and viruses. As an example, Ghatak, *et al.*[1] have shown that a weak electric field (0.5 V) generated by an electroceutical fabric can disrupt the infectivity of coronavirus upon contact by destabilizing the electrokinetic properties of the virion. However, a limitation of this method is that the fabric needs to be wetted by an aqueous electrolyte or bodily fluids to generate the electrical field. The same electric field is found to be disruptive against different bacteria and biofilms and suitable for preventing wound infections.[25,35,38]

It has also recently been discovered that capacitive materials can deactivate bacteria after being charged in the presence of a direct or alternating current (DC, AC).[2,37] Such materials can sustain their antibacterial and antiviral properties after the withdrawal of the power supply by discharging the stored charge.[2,37,39] Wang, *et al.*[2] have developed carbon-doped titania nanotubes with tunable capacitance, which exhibited a sustained antibacterial effect after withdrawal of the power supply in a bacterial suspension. In our previous study, we developed laser-scribed graphene (LSG) electrodes that could be charged in a saline solution with a low constant potential of 1–2 V.[33] These capacitive electrodes have been shown to exhibit sustained antibacterial and antiviral properties after being unplugged from 10 minutes of charging in an aqueous electrolyte. Our research showed a direct relationship between the capacitance and the antibacterial and antiviral properties of the LSG electrodes.[33]

All the studies mentioned so far share a common drawback: the requirement for an aqueous electrolyte during the charging process of capacitive surfaces, which limits their potential applications. In this study, we aimed to overcome this limitation by investigating the potential of a solid-state symmetric supercapacitor that eliminates the need for a liquid electrolyte. As a result, our study introduces new properties and applications for the extensively studied technology of supercapacitors by exploring their antibacterial and antiviral capabilities. We proposed a new concept of antibacterial and antiviral supercapacitors and developed symmetric electrical double-layer supercapacitors comprising two parallel layers of carbon cloth (CC) electrodes, a solid polymer electrolyte and a separator. The electrochemical characteristics of the carbon cloth (CC) electrodes and carbon cloth solid-state supercapacitor (CCSC) and their capacitance-related antibacterial and antiviral properties were studied. Recent advances in flexible and self-healing supercapacitors have primarily focused on developing new materials and designs, such as graphene, conducting polymers, and hydrogels.[40–44] These materials offer improved energy storage capabilities and mechanical flexibility.[43] In addition, innovative approaches like nanocomposite films and 3D printing techniques have been utilized to create flexible electrode structures that exhibit enhanced conductivity and stability.[45,46] These significant advancements have paved the way for the development of flexible supercapacitors, which are poised to revolutionize next-generation wearable electronics and flexible energy storage applications.[47] Moreover, the incorporation of antibacterial properties into such technologies has the potential to unlock a wide range of diverse applications. To the best of our knowledge, there has been no study reported before on the antibacterial and antiviral properties of a solid-state supercapacitor material. This technology can be considered a new generation of environmentally friendly antibacterial and antiviral platforms that provides a broad range of sustainable biocidal activities with lower power requirements. Innovations in the design of supercapacitors, such as adding antibacterial and antiviral features, can lead to numerous applications in wearable electronics, biomedical applications and e-skin devices for health monitoring and infection prevention.[11,48]

Experimental section

Materials

Poly(vinyl alcohol), M_w 146 000–186 000, 99+% hydrolyzed, was purchased from Sigma-Aldrich (New Zealand). Glycerol and sodium chloride (NaCl, Analytical Reagents Grade (AR)) were purchased from ECP limited. Carbon cloth ELAT – Hydrophilic Plain Cloth (Woven Carbon Fiber) was purchased from the Fuel Cell Store. The bacterial strain, *Escherichia coli* ATCC 25922, was purchased from the American Type Culture Collection through Cryosite, Australia. Bacterial growth media Difco Cation-Adjusted Mueller Hinton Broth (MHB) and Agar (MHA) were purchased from Fort Richard (Auckland). Tween 80 was purchased from Sigma. Vero cells were from ATCC CCL-81, and HSV-1 virus was provided from Westmead Institute for medical research, NSW, Australia. Cell growth media Gibco Dulbecco's Modified Eagle Medium (DMEM), Gibco Fetal Bovine Serum (FBS), and 1× penicillin–streptomycin (PS) were purchased from Thermo Fischer. Carboxymethyl cellulose (Sigma-Aldrich) was used for cell overlay. All reagents and materials were used without further purification. All aqueous solutions were prepared using deionized water (Milli-Q, 18.2 MΩ cm). Phosphate buffer solution (PBS) and other chemicals in this study were of analytical grade and were used as supplied.

Preparation of solid polymer electrolyte

Solid electrolytes are more stable than liquid electrolytes and can be more practical for the multilayer design of antibacterial

This journal is © The Royal Society of Chemistry 2023

J. Mater. Chem. B, 2023, **11**, 8170–8181 | **8171**

and antiviral supercapacitors. Therefore, a polyvinyl alcohol (PVA) hydrogel with a neutral salt (NaCl) was selected here as a 'green' material for the polymer electrolyte. PVA (4.0 g) was dissolved in 60 mL of distilled water in a flask under stirring at 95 °C and mixing (500 rpm) for 2 h until it completely dissolved and formed a jelly-like solution. The calculated amount of NaCl was dissolved in 15 mL of distilled water. Glycerol and the dissolved NaCl were added to the PVA solution under stirring (500 rpm) at 90 °C. The optimized solid polymer electrolyte composition consisted of PVA, NaCl, and glycerol in a weight ratio of 1 : 0.8 : 1. The bubbles were removed from the solution by 5 min ultrasonication. The obtained PVA/glycerol/NaCl solution was allowed to cool down and stored at room temperature.

Assembly of symmetrical CC supercapacitor

We selected a CC material that consists of uniform-size carbon fibers in a woven porous structure. Two pieces of CC, with a dimension of 1 × 3 cm, were cut and used as positive and negative electrodes. The as-prepared CC pieces and a piece of filter paper were immersed in the prepared gel electrolyte, consisting of PVA, NaCl, glycerol and water, for 3 minutes to allow soaking of the electrolyte into the porous structure of the CC. The electrodes were assembled according to the scheme in Fig. 1 with an active supercapacitor working area of 2.5 cm² consisting of two CC electrodes (anode and cathode), sandwiching PVA/glycerol/NaCl polymer electrolyte and a filter paper as a separator. The assembled supercapacitor device was dried at room temperature for 24 h, affording a solid-state carbon cloth supercapacitor (CCSC).

Characterization

Scanning electron microscopy (SEM) was conducted using a FEI Phillips XL30 S-FEG instrument. Cyclic voltammetry (CV) measurements were conducted in a three-electrode setup, with the CC (2 cm² dimension and an active surface area of 4 cm² since both sides of CC take part in the electrochemistry) as the working electrode, in the saline solution (0.9% w/v sodium chloride solution) at room temperature, using a PalmSense4 Potentiostat. A platinum wire was used as a counter electrode and Ag/AgCl in 3 M KCl as a reference electrode (0.210 V vs. SHE). Resistance and conductivity of CC electrodes was measured using a four-point probe conductivity meter (Janel RM2), taking an average of 5 points per electrode. The electrodes'

water contact angle (WCA) measurements were determined by imaging a droplet of deionized water on the surfaces using a CAM100 KSV setup. The images were analyzed by CAM100 KSV software in an auto-calculation mode.

The carbon cloth solid-state supercapacitor's electrochemical performance was investigated by CV and galvanostatic charge–discharge (GCD) experiments in a two-electrode setup. The CV measurements were undertaken over different potential ranges at different scan rates from 1 to 1000 mV s^{-1}. The GCD curves were measured in the potential range of 0 to +1 V at current densities of 0.027 mA cm^{-2} to 1.33 mA cm^{-2}. The cycling performance was tested by CV sweeps at a scan rate of 100 mV s^{-1} for 1000 cycles in a potential range of 0 to 1 V.

The areal specific capacitance of the CCSC device was calculated from the CV curves obtained at different scan rates in the potential window of 0 to +1 V. Areal capacitance of the electrodes, as a function of the scan rate, was calculated according to eqn (1)[49]:

$$C_A = \frac{1}{A\Delta U\, S}\left(\int I(U)\mathrm{d}U\right) \qquad (1)$$

where C_A is the areal capacitance, A (cm²) is the nominal area of the electrode, ΔU is the potential window, S is the scan rate, and $I(U)$ is the current of the discharge curve integrated with respect to the potential U.

Preparation and charging of electrodes prior to antibacterial and antiviral testing

A non-antimicrobial polyimide (PI) sheet was cut into 1 × 1 cm² squares and used as control samples. The samples were sterilized by sequential 1 minute immersions in 100%, 70%, and 100% ethanol before air drying in a biological safety cabinet before use. The CC samples were charged at either +1.5 or −1.5 V vs. Ag/AgCl reference electrode for 10 min in saline solution (0.9% NaCl in water) in a three-electrode setup with a platinum wire as the counter electrode and an Ag/AgCl reference electrode. The charged and noncharged samples were unplugged, and CC samples were removed from the saline solution and dried. The CCSCs were charged at either +1.5 or −1.5 V for 10 min in a two-electrode setup, using a portable PalmSense Potentiostat.
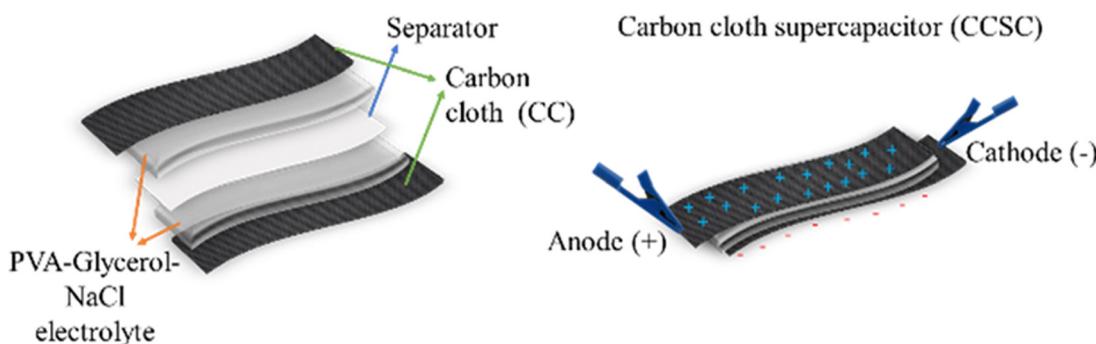

Fig. 1 Schematic illustration of the assembling process of the flexible, solid-state symmetric carbon cloth supercapacitor (CCSC) devices.

Antimicrobial properties of the CC and CCSC

The antimicrobial properties of CC and CCSC were tested against *E. coli* using a modified version of the Japanese Industrial Standard (JIS 2801:2010) assay.[50] 10 mL bacterial overnight suspension containing 10^9 colony-forming units (CFU) mL^{-1} of *E. coli* was prepared in MHB medium at 37 °C and then were diluted into saline to a concentration of approximately 10^8 CFU mL^{-1}.

10 μL of the test inoculum (approximately 10^6 CFU) was inoculated to the surface of each sample. All the samples were incubated for 1 h. After incubation, the samples were placed into a sterile centrifuge tube with 10 mL of MHB broth +1% v/v tween 80. The tubes were vortexed vigorously every 5 min to release the viable bacteria remaining on the samples to the wash solution. The obtained wash solution has been used for live/dead bacteria imaging and bacterial enumeration. The surviving cells were enumerated as colony-forming units (CFUs) by (a) plating 100 μL aliquots of the wash solution onto Mueller Hinton agar (MHA); (b) plating 100 μL of a mixture of 10 μL wash solution diluted with 990 μL sterile saline solution; and (c) pour plates of the remaining wash solution (approximately 10 mL) mixed with 10 mL molten (55 °C) MHA. Surviving cells were enumerated as CFUs on the MHA plates with 10–300 colonies after incubation at 37 °C for 24 to 48 h.

SEM and live/dead bacteria staining imaging

The bacteria solution containing 10^7 CFU of *E. coli* was added onto the noncharged and charged CCSCs and these were incubated in the dark at 37 °C for 1 h. The samples were then immersed in 2.5% glutaraldehyde overnight and treated with gradient alcohol (10, 30, 50, 70, 90 and 100%) for 10 min each and dried. The samples were then put on a specimen stage prior and coated with platinum for 60 s (thickness 10 nm). Images of the bacteria were obtained using a Hitachi SU-70 scanning electron microscope (SEM).

For live/dead staining imaging, a combination of Syto9 and PI stains was prepared by adding 1 μL of each dye into 1 mL of saline solution. 10 μL of wash solution was mixed with 10 μL of dye mix and then deposited on a slide and kept in the dark for 15 minutes prior to the imaging. The live/dead bacteria imaging was performed using a Zeiss Axio Imager M2 fluorescence microscope. The bacteria stained with SYTO-9 (green) were imaged using a GFP filter, and dead bacteria stained with PI (red) were imaged using a Texas Red filter.

Antiviral properties against HSV-1

The antiviral activity of carbon cloth solid-state capacitors (CCSC) subjected to different charging voltages was assessed against herpes virus HSV-1 which is a double-stranded DNA virus used as a surrogate for SARS-CoV-2.[51]

10 μL of virus stock containing 2×10^7 plaque-forming units (PFU) was applied to one side of the CCSC and left for 20 min. Samples were then immersed in 2 mL of growth media (DMEM with 10% FBS) and vortexed every 5 min for 30 min before CCSC samples were removed and liquid samples were stored at −80 °C prior to plaque and qPCR assays. Viral titre was measured by a plaque assay after infection of Vero cells with

serial dilution of the samples.[52] Briefly, 300 μL of 10-fold serial dilutions of virus-containing samples were applied to Vero cells grown in 12 well culture dishes. The virus inoculum was removed after 2 h, and the cells were overlaid gently with 1 mL DMEM containing 10% FBS and 0.25% methylcellulose. Plates were incubated for 2 days when the medium was removed, and plaques were stained with 0.1% crystal violet (in 20% methanol).

Quantitative polymerase chain reaction (qPCR)

Viral DNA was recovered from 1/10th of the wash solutions using Zymo Research Quick-DNA 96 kit. Viral genome copy number in each sample was assessed by qPCR using primers specific for HSV-1 ICP47 (forward 5′-TCGTGCACGGCGGTTCTG-3′ and reverse′-ACCTTCCTGGACACCATGCG-3′), as described by Garvey, *et al.*[53] The specificity of amplification was confirmed by melting curve analysis. For each PCR, the cycle threshold (C_t) corresponding to the cycle where the amplification curve crossed the baseline was determined.

Statistical analysis

GraphPad Prism (GraphPad Software) v8.0 was used for statistical analyses. Statistical analysis between multiple groups was performed using one-way analysis of variance (ANOVA), and the significant differences were assessed by Duncan's multiple range test (at $p < 0.05$). The data are reported as means ± standard deviations (SD). Statistical analysis for biological assays was performed using GraphPad Prism v8.0.2 software, and the results are reported as the means with range.

Results and discussion

Electrochemical characterization of CC electrodes and CCSCs

Fig. 2A–D depicts surface SEM images of carbon cloth electrodes taken before and after the gel polymer electrolyte was cast.

The CCSCs devices were assembled as depicted in Fig. 1 and optimized (details provided in ESI†). The cyclic voltammetry characterization of CC electrodes (Fig. 3A) and CCSC device (Fig. 3B) was undertaken in the potential range of 0 to 1 V (at a scan rate of 100 mV s^{-1}). The CC showed a low areal capacitance of 0.75 ± 0.06 mF cm^{-2}, which is in agreement with the reported areal capacitance value for a commercial carbon cloth.[36] The electrical conductivity and sheet resistance of CC electrodes were about 79 ± 11 S cm^{-1} and 1 ± 0.39 Ω cm^{-1}, respectively. The semi-rectangular CV shape of the CC with no faradaic redox peaks suggests that the current is mainly due to electric double-layer capacitance (EDLC) (Fig. 3A).[54,55]

Notably, recent reports have shown that porous carbon materials, including unmodified carbon cloth, have relatively low energy density and specific capacitance, making them unsuitable for high-energy electronic devices.[56–59] To enhance the specific capacitance of these materials, various methods have been employed, such as coating with pseudocapacitive materials like transition metal oxides and conductive polymers, or activating the carbon through thermal, acid, electrochemical, or plasma treatments.[42,57–59] However, the objective of our current

This journal is © The Royal Society of Chemistry 2023

J. Mater. Chem. B, 2023, **11**, 8170–8181 | 8173
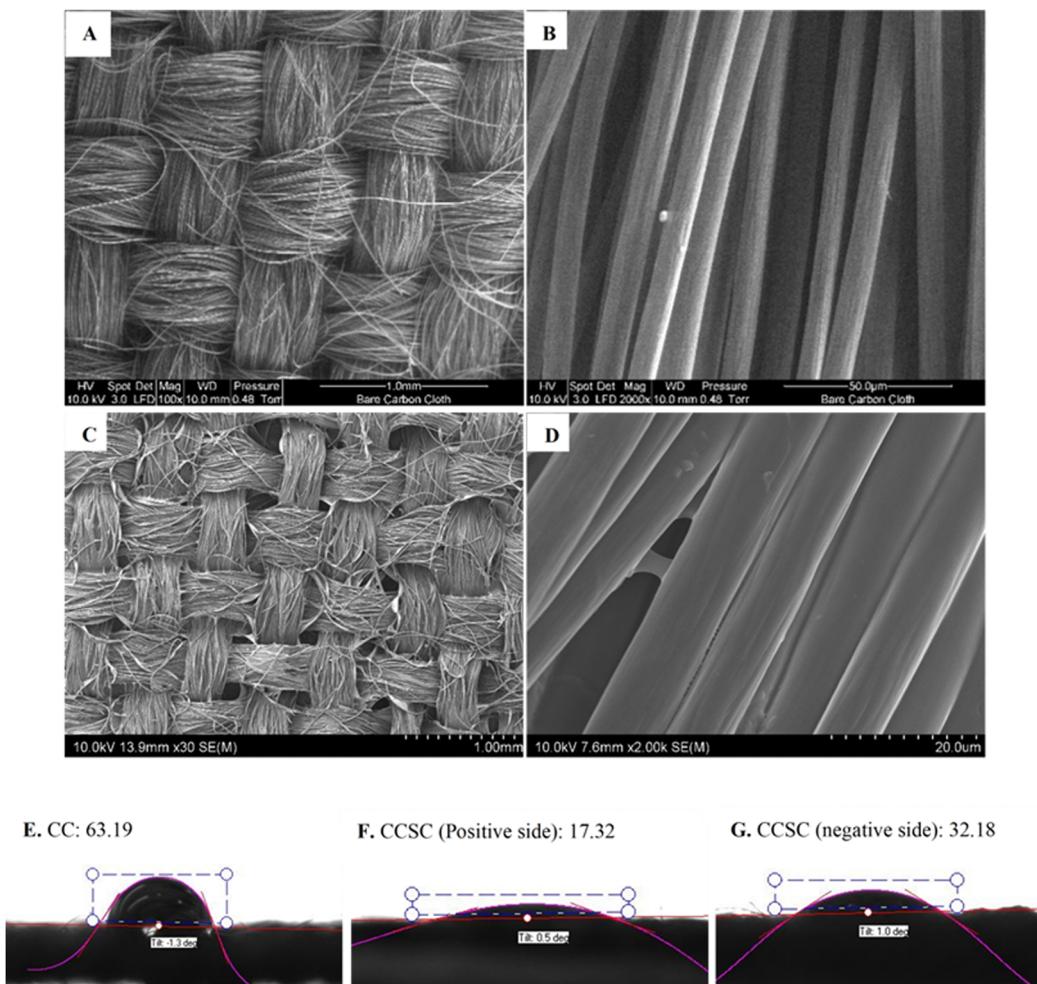
Fig. 2 (A and B) SEM micrographs of ELAT hydrophilic carbon cloth at different magnifications; (C and D) SEM micrographs of assembled CCSC surface; the water contact angle of: (E) CC, (F) positive side of CCSC and (G) negative side of CCSC.

study was not to achieve high capacitance, but rather to demonstrate that porous carbon materials can exhibit sufficient capacitance for the disinfection of harmful bacteria and viruses. To achieve this, we chose to use unmodified carbon cloth as our material of choice, due to its simple preparation method.

CV curves of the CCSC were collected under various bending and twisting conditions at a scan rate of 100 mV s^{-1} (Fig. 3B), demonstrating the flexibility and bendability of the CCSC. Such properties are desirable for flexible and wearable electronic device applications,[56,60,61] and the results here suggest possible uses of the fabricated CCSC in such applications. Fig. 3C displays the CV profile of CCSCs at the scan rate of 100 mV s^{-1} and over different potential windows. The CV profiles of CCSCs showed nice symmetrical rectangular shapes with no prominent redox peaks within the potential window of -1 to 1.3 V (Fig. 3C). The edge of the CV shape was elongated, or the current curved upward when the potential window was increased to more than 1.3 V, which could be attributed to the generation of oxidizing species, such as hydroxyl radicals, and CO-type surface groups, such as the incorporation of carbonyl or quinone surface group (Fig. 3C).[62,63] The rectangular CV curves of CCSC within the wide potential

window of -1 to 1.3 V showed that the device has good charge storage and high-power capability (Fig. 3C). The results show that the areal capacitance of the CCSCs increased by extending the potential window (Fig. S.2E, ESI†). The areal capacitance of the CCSCs increased by 54% from 4.2 ± 0.2 mF cm^{-2} in the potential window of 0 to $+1$ V to 6.4 ± 0.4 mF cm^{-2} in the potential window of 0 to $+2$ V (Fig. S.2E, ESI†). The increase in the capacitance could be attributed to the generation of CO-type surface groups upon anodic polarization and wettability improvement of carbon surface due to the incorporation of oxygenated groups, also supported by the WCA measurements (Fig. 2E–G).[62–64] A lower WCA indicates a higher contact area between the surface of the electrode and the aqueous solutions, which could result in a faster charge conveyance.[65] The WCA results showed that the average water contact angle of the CC electrodes was 63.19°, and the CCSCS showed better wettability and a lower contact angle (Fig. 2E–G).

The CV profile of the CCSCs device, in the scan rate range of 2–500 mV s^{-1}, was collected in the potential window from 0 to 1 V (Fig. 3D). All CV curves retained their symmetrical rectangular shape at all scan rates, indicating the excellent double-layer capacitive performance, low contact resistance and high-power

8174 | *J. Mater. Chem. B*, 2023, **11**, 8170–8181

This journal is © The Royal Society of Chemistry 2023
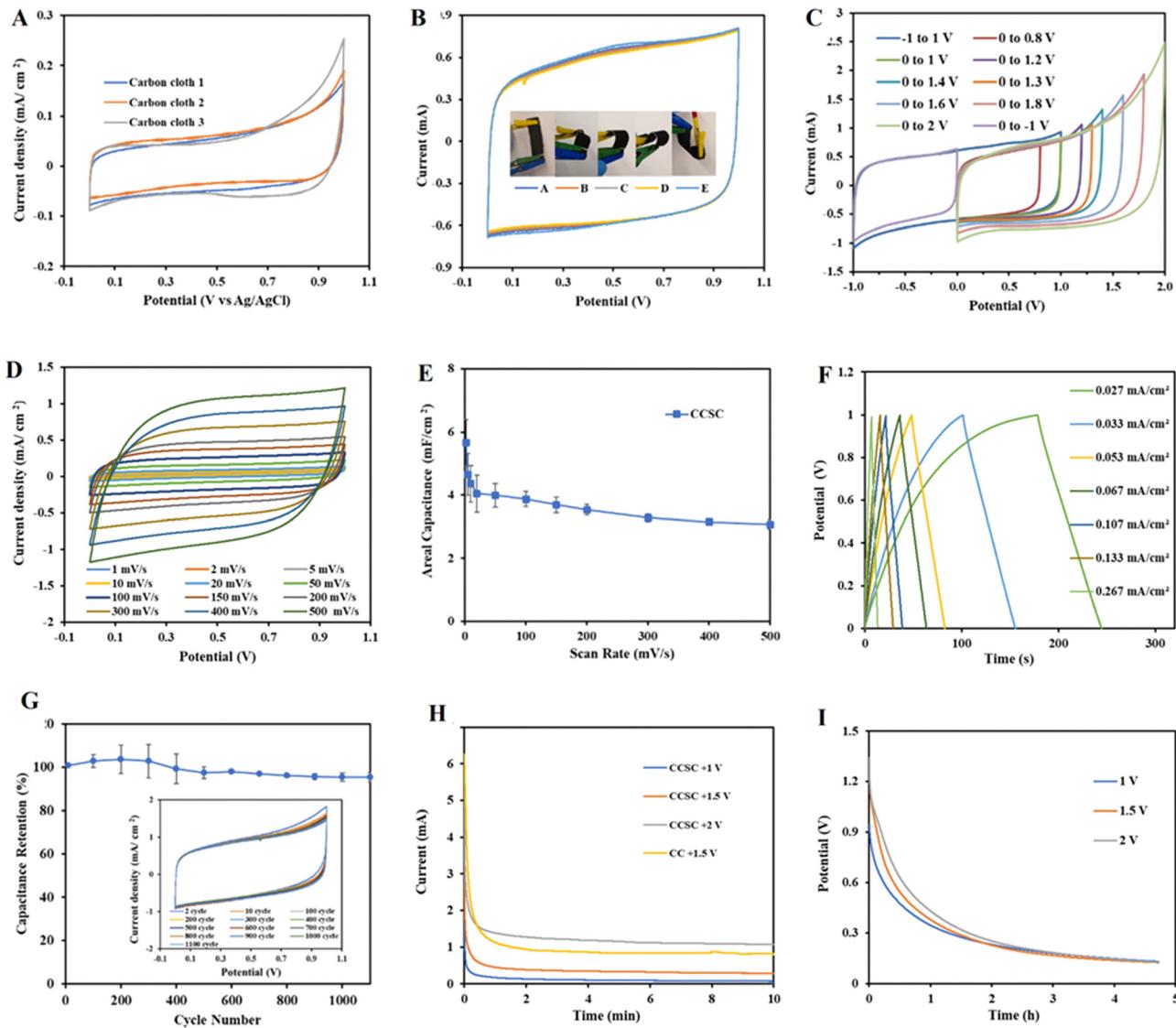
Fig. 3 (A) CV curves of CC electrodes (surface area of 1.5 cm^2) in a three-electrode setup in saline solution (0.9 wt% NaCl) at a scan rate of 100 mV s^{-1}; (B) CV curves of CCSCs under different bent and twisted conditions at a scan rate of 100 mV s^{-1}. (C) CV curves of CCSCs at a scan rate of 100 mV s^{-1}, in different potential windows. (D) CV curves of the CCSC under scan rates in the range of 2–500 mV s^{-1} within the potential window of 0 to 1 V. (E). The average areal capacitance of CCSC as a function of scan rate (n = 3). (F) Galvanostatic charge–discharge (GCD) analysis of CCSC in the potential range of 0 to +1 V. (G) Percentage of average areal capacitance retention of CCSCs as a function of cycle number, along with the CV scans at the scan rate of 100 mV s^{-1} in the potential window from 0 to +1 V (n = 3). (H) Choroamperograms (CA) of a CC electrode and the CCSCs device by applying constant potentials of +1, +1.5 and +2 V for 10 min, (I) open-circuit potential (OCP) of the CCSCs for 5 h after being charged with constant potentials of +1, +1.5 and +2 V.

capability of the CCSCs. The average areal capacitance of CCSCs, calculated from CV curves, as a function of the scan rate, is shown in Fig. 3E, calculated from the CV curves shown in Fig. 3D. Capacitance retention at higher scan rates is desirable for supercapacitors in various applications.[57,66] The results showed that the areal capacitance of CCSCs gradually decreased with the increase in the scan rate. Such decrease is related to diffusion limitations of electrolyte in pores of electrode material.[33,67,68] However, 83% of the areal capacitance calculated from the CV obtained at the scan rate of 5 mV s^{-1} was preserved at the scan rate of 100 mV s^{-1}, indicating a good high-rate capability of the CCSCs (Fig. 3E).

Furthermore, galvanostatic charge–discharge (GCD) tests were carried out in the positive potential range from 0 to +1 V, at various current densities (Fig. 3F). The GCD profile of CCSC showed symmetrical triangular shapes, indicating excellent device capacitive performance, fast and reversible charge/discharge performance, and good cycling stability (Fig. 3F). No IR drop was recorded for the discharge curves, implying negligible resistance, excellent electrochemical reversibility, and high conductivity for the CCSCs electrodes (Fig. 3F). Fig. 3G displays the excellent long-term electrochemical cycling stability of the CCSCs, with CCSCs exhibiting 97% retention of the initial areal capacitance after 1000 cycles.

The CC electrodes and the CCSCs were charged by applying different constant potentials for 10 min. In chronoamperometry mode (Fig. 3H), different constant potentials of +1, +1.5, and +2 V were applied, and the currents were recorded for 10 mins. The current drop showed an approximately exponential behavior indicating the charging characteristics of double-layer capacitors. The current densities for all samples dropped rapidly initially, reached the steady-state within about 20 s, and remained at the steady-state currents for the duration of the experiment (Fig. 3H). As double-layer charging occurs fast, the ongoing and declining current at steady-state might be due to the background carbon oxidation (faradaic processes), and at higher potentials to electrolyte oxidation and generation of chlorine species.[63] It was also observed that with the increase in charging potential, the curves and the steady-state currents move up without much change in the shape of the curves (Fig. 3H). Integrating the I–t curves provides the total charge passed, which increased with the increase in the charging potential.[33] The total charges for CCSCs were 73, 213 and 730 mC for the charging potential of +1, +1.5 and +2 V, respectively. Increasing the charging potential from +1 to +1.5 V increased the total charge by about 3 times (Fig. 3H).

The open-circuit potential (OCP) data were monitored to study the loss of the surface potential of the CCSCs device charged to +1, 1.5 and +2 V, during a period of 5 h (Fig. 3I). The initial potentials of CCSCs were lower than the constant potential applied during charging, and the initial surface potential decay was rapid, followed by a more gradual decrease in potential (Fig. 3I). The potential of CCSCs charged at different constant potentials was initially distinct and proportional to the applied charging potential (Fig. 3I). The results showed that the discharge rates of the CCSCs were greater with an increase in the charging potential (Fig. 3I).

Antibacterial performances of CC electrodes and CCSCs device

The antibacterial performances of the CC electrodes and the CCSCs device, charged by applying a constant potential of $\pm$ 1.5 V for 10 min, were studied. A modified standard assay (JIS Z 2801) to test antibacterial properties was applied against *E. coli*. Antibacterial test results, after 1 h of incubation time with the bacteria on the surface of CC electrodes and CCSCs device, are shown in Fig. 4A. Not charged (NC) CC electrode and CCSC device displayed no antibacterial effect against *E. coli*, eliminating any antibacterial effect of the CC material and allowing attribution of any antibacterial properties observed to the charged properties of the electrode and the charged devices (Fig. 4A). The electrochemical analysis of CC showed that the electrodes had a low capacitance of 0.7 mF cm^{-2}, while their antibacterial efficacy assay showed 3 and 2 logs reduction of *E. coli* inocula, for positively and negatively charged samples, respectively (Fig. 4A).

Charged CCSCs caused more than 5 log reduction of *E. coli* inocula, confirming the capacitance-base antibacterial effect of the device (Fig. 4A). The positively charged side of CCSC resulted in 100% deactivation of bacteria within 1 h incubation time of the bacteria. The antibacterial performance of the charged CCSCs samples was further verified by the SEM and live/dead bacteria imaging (Fig. 5). SEM images were obtained of the fixed bacteria
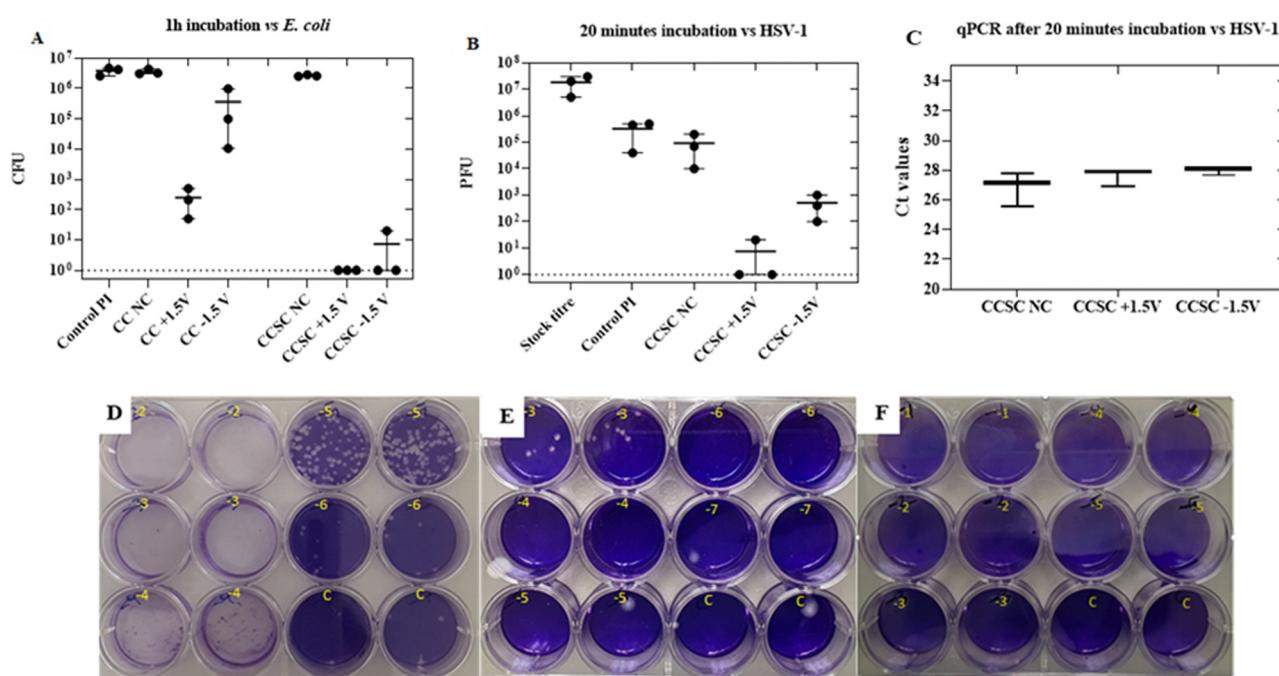

Fig. 4 (A) Antibacterial assay results for charged CC electrode and charged CCSCs device against *E. coli* after 1 h of incubation (B) antiviral assays results for the CCSC device against HSV-1 herpes virus after 20 min of incubation time. Antibacterial and antiviral assays were performed in triplicate on three occasions. (Each point in Figures A and B represents the means of each biological run. The wide bar represents the means of three independent experiments. Error bars represent the range of values obtained). (C) C_t values of the eluted virus particles from noncharged and charged CCSC samples. The wide bar represents the medians and the error bars represent the range of values obtained. (n = 3) (D) Plaque assay results for stock titre of herpes virus suspension. (E) Plaque assay results for not charged CCSCs (CCSC NC). (F) Plaque assay results for charged CCSC with +1.5 V potential (CCSC +1.5 V).

on charged and noncharged CCSCs after 1 h incubation time to investigate the bacterial morphological changes (Fig. 5B). The bacteria cultured on noncharged CCSCs exhibited a high concentration and aggregation of bacteria (Fig. 5B). The density of *E. coli* was much lower on the positively and negatively charged sides of CCSCs, which could be attributed to the severe damage of bacterial cell membrane and, subsequently, severe disintegration

of the cells (Fig. 5B). Surface charge transfer and charge-induced oxidative stress can damage bacterial cell walls, disrupting bacterial respiration and leading to bacterial death.[22,69] The morphology of bacteria on charged samples was distorted, broken and wrinkled, indicating that the intracellular content had leaked out (Fig. 5B). The live/dead staining results were in good agreement with the colony forming unit (CFU) counting results
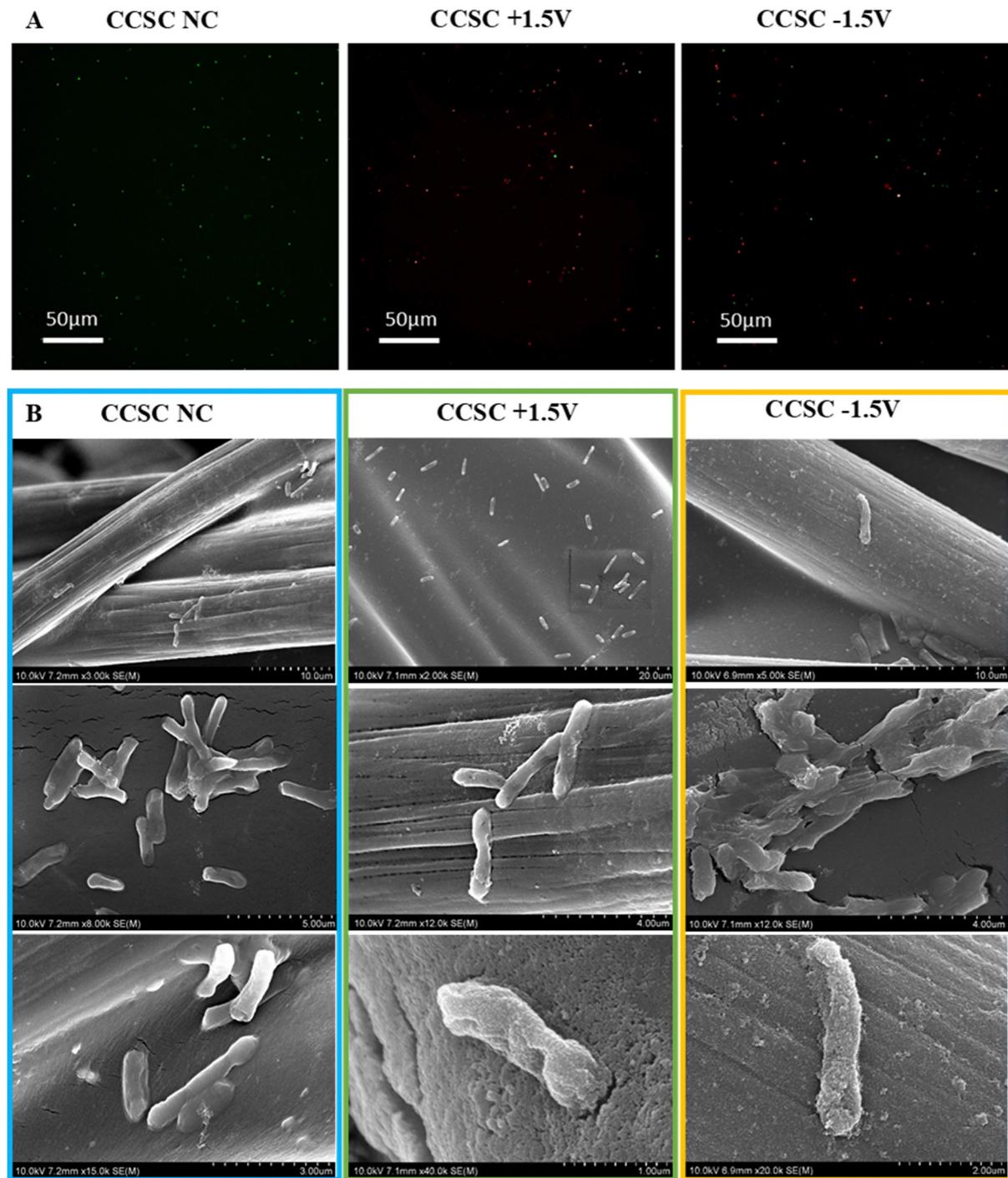

Fig. 5 (A) Live/dead imaging of *E. coli* of wash solutions after 1 h incubation onto the noncharged and charged CCSC samples, (B) scanning electron microscopy (SEM) images of *E. coli* on noncharged and charged CCSC samples.

presented in Fig. 4A. Bacteria washed from the noncharged samples appeared fluorescent green indicating live cells (Fig. 5A). By contrast, red cells were observed for the charged CCSCs (Fig. 5A). Inconsistent with the colony counting results, a few live cells were detected in the charged samples which could be explained by the viable but non-culturable state of bacteria after being treated with the charge surface (Fig. 5A).

Antiviral capacitance-dependent performance of CCSC device

The antiviral performance of the CCSCs device, subjected to different charging potentials, was assessed by a plaque assay method against Herpes simplex virus 1 (HSV-1).[52] The stock titre of the herpes virus for the experiment was $\sim 10^7$ PFU (Fig. 4D). Inert polyimide (PI) sheets were used as control samples.

The control and noncharged CCSC samples displayed a similar plaque count, about $\sim 10^5$ PFU, after 20 min incubation time (Fig. 4B and E). The reason behind the fold change from the initial stock concentration of 10^7 to 10^5 in the control samples is due to the washing step of infected samples in 2 mL of growth media during the plaque assay (Fig. 4B). The positively and negatively charged CCSCs showed approximately 5 and 2 log reductions in PFU, respectively (Fig. 4B). The qPCR has been used to detect and quantify the virus DNA in clinical samples in many studies.[70–72] The C_t (cycle threshold) is defined as the number of cycles required for the fluorescent signal to cross the threshold which is inversely proportional to the amount of target nucleic acid in the sample.[70] The qPCR was performed on the wash solutions that we prepared for the HSV-1 antiviral plaque assay to confirm that the virus particles were eluted from the surface to the wash solution and have not bounded to the charged surfaces. There was no significant difference ($p > 0.05$) between the obtained C_t values for the not charged, positively and negatively charged samples wash solutions indicating that similar quantities of virus particles were desorbed from each charged surface following exposure (Fig. 4C). The qPCR results confirm that the reduction in the titre of infectious HSV-1, following surface contact, was due to physico-chemical alteration of the virus structure and loss of its infectivity and not to the retention of particles on the surface material. Based on these results, the antiviral properties of the charged devices could be attributed solely to the charging of the device and to the disruption of the structural integrity of the herpes virus by a low voltage electric current.[1,11,34,73] It has also been reported in other studies that the low voltage electric currents can damage the bilayer envelop membrane of the virus and hence inhibit its infectivity.[1,33,73]

The infectivity of virions, or the capability of viruses to enter host cells and reproduce, depends on their structural stability and assembly.[1,7] We can attribute the antiviral effect of the stored charge on CCSCs to the disruption of the electrokinetic assembly of virions and electroporation of the membrane or capsid.[1,35,73,74] It also has been reported in other studies that the low current density and electric field at low voltages could lead to electrostatic interactions destructing viral structures and/or inhibiting viral infection pathways.[35,74,75]

Conclusions

In conclusion, this study presents a novel concept of utilizing supercapacitors not only as energy storage devices, but also as active, post-charging, antibacterial, and antiviral devices. The flexible, solid-state supercapacitors fabricated in this study, based on carbon cloth and PVA–glycerol–NaCl electrolyte, exhibited promising performance for flexible and wearable charge storage applications. The CCSCs showed excellent rate capability, retaining 97% of the initial capacitance after 100 cycles. Moreover, charging the CCSCs with a low voltage of +1.5 V was sufficient for 6 log removal of *E. coli* and 5 log removal of herpes simplex virus HSV-1, demonstrating the antibacterial and antiviral properties of the supercapacitors. The findings of this study highlight the potential of supercapacitors as multifunctional devices with not only energy storage capabilities, but also antibacterial and antiviral properties. This research contributes to the understanding of the unexplored field of using supercapacitors for antimicrobial applications, opening new possibilities for the development of advanced materials for various biomedical and environmental applications.

Conflicts of interest

There are no conflicts to declare.

Acknowledgements

Notes and references

1 S. Ghatak, *et al.*, Electroceutical fabric lowers zeta potential and eradicates coronavirus infectivity upon contact, *Sci. Rep.*, 2021, **11**, 1–11.

2 G. Wang, *et al.*, An antibacterial platform based on capacitive carbon-doped TiO_2 nanotubes after direct or alternating current charging, *Nat. Commun.*, 2018, **9**, 1–12.

3 E. Kolanthai, C. J. Neal, U. Kumar, Y. Fu and S. Seal, Antiviral nanopharmaceuticals: engineered surface interactions and virus-selective activity, *Wiley Interdiscip. Rev.: Nanomed. Nanobiotechnol.*, 2022, e1823.

4 M. A. Sadique, *et al.*, High-performance antiviral nanosystems as a shield to inhibit viral infections: SARS-CoV-2 as a model case study, *J. Mater. Chem. B*, 2021, **9**, 4620–4642.

5 C.-M. Chiu, *et al.*, Self-powered active antibacterial clothing through hybrid effects of nanowire-enhanced electric field electroporation and controllable hydrogen peroxide generation, *Nano Energy*, 2018, **53**, 1–10.

6 T. Zhang and P.-L. Tremblay, Graphene: an antibacterial agent or a promoter of bacterial proliferation?, *Iscience*, 2020, **23**, 101787.

7 X. Zou, L. Zhang, Z. Wang and Y. Luo, Mechanisms of the antimicrobial activities of graphene materials, *J. Am. Chem. Soc.*, 2016, **138**, 2064–2077.

8 A. Al-Jumaili, S. Alancherry, K. Bazaka and M. V. Jacob, Review on the antimicrobial properties of carbon nanostructures, *Materials*, 2017, **10**, 1066.

9 H. E. Karahan, *et al.*, Graphene materials in antimicrobial nanomedicine: current status and future perspectives, *Adv. Healthcare Mater.*, 2018, **7**, 1701406.

10 L. Giraud, A. Tourrette and E. Flahaut, Carbon nanomaterials-based polymer-matrix nanocomposites for antimicrobial applications: a review, *Carbon*, 2021, **182**, 463–483.

11 M. Ayub, M. H. D. Othman, I. U. Khan, M. Z. M. Yusop and T. A. Kurniawan, Graphene-based nanomaterials as antimicrobial surface coatings: a parallel approach to restrain the expansion of COVID-19, *Surf. Interfaces*, 2021, **27**, 101460.

12 H. Wang, *et al.*, Carbon dots with positive surface charge from tartaric acid and m-aminophenol for selective killing of Gram-positive bacteria, *J. Mater. Chem. B*, 2021, **9**, 125–130.

13 H. Le Pape, *et al.*, Evaluation of the anti-microbial properties of an activated carbon fibre supporting silver using a dynamic method, *Carbon*, 2002, **40**, 2947–2954.

14 H. Tamai, N. Katsu, K. Ono and H. Yasuda, Antibacterial activated carbons prepared from pitch containing organometallics, *Carbon*, 2001, **39**, 1963–1969.

15 P. Anjana, M. Bindhu, M. Umadevi and R. Rakhi, Antibacterial and electrochemical activities of silver, gold, and palladium nanoparticles dispersed amorphous carbon composites, *Appl. Surf. Sci.*, 2019, **479**, 96–104.

16 A. Bahadoran, *et al.*, Co-doping silver and iron on graphitic carbon nitride-carrageenan nanocomposite for the photocatalytic process, rapidly colorimetric detection and antibacterial properties, *Surf. Interfaces*, 2021, **26**, 101279.

17 S. Szunerits and R. Boukherroub, Antibacterial activity of graphene-based materials, *J. Mater. Chem. B*, 2016, **4**, 6892–6912.

18 C. Monteserín, *et al.*, Novel antibacterial and toughened carbon-fibre/epoxy composites by the incorporation of TiO_2 nanoparticles modified electrospun nanofibre veils, *Polymers*, 2019, **11**, 1524.

19 E. Zhang, *et al.*, Antibacterial metals and alloys for potential biomedical implants, *Bioactive Mater.*, 2021, **6**, 2569–2612.

20 M. Yang, *et al.*, Electron transfer correlated antibacterial activity of biocompatible graphene nanosheets-TiO_2 coatings, *Carbon*, 2020, **166**, 350–360.

21 N. F. Attia, A. Mohamed, A. Hussein, A.-G. M. El-Demerdash and S. H. Kandil, Greener bio-based spherical nanoparticles for efficient multilayer textile fabrics nanocoating with outstanding fire retardancy, toxic gases suppression, reinforcement and antibacterial properties, *Surf. Interfaces*, 2023, **36**, 102595.

22 W. Zhou, *et al.*, Construction of high surface potential polypyrrole nanorods with enhanced antibacterial properties, *J. Mater. Chem. B*, 2018, **6**, 3128–3135.

23 S. P. Singh, *et al.*, Laser-induced graphene layers and electrodes prevents microbial fouling and exerts

antimicrobial action, *ACS Appl. Mater. Interfaces*, 2017, **9**, 18238–18247.

24 L.-N. Wu, *et al.*, Levofloxacin-based carbon dots to enhance antibacterial activities and combat antibiotic resistance, *Carbon*, 2022, **186**, 452–464.

25 L. Shi, *et al.*, Antibacterial and osteoinductive capability of orthopedic materials via cation–π interaction mediated positive charge, *J. Mater. Chem. B*, 2015, **3**, 733–737.

26 P. H. Carey IV, *et al.*, Antibacterial Properties of Charged TiN Surfaces for Dental Implant Application, *ChemistrySelect*, 2019, **4**, 9185–9189.

27 Z. Zhang, *et al.*, Fabrication of antibacterial Janus bandages with high wound healing performances by facile single-side electrospray PDMS coating, *Surf. Interfaces*, 2022, **34**, 102392.

28 X. Li, *et al.*, Recent developments in smart antibacterial surfaces to inhibit biofilm formation and bacterial infections, *J. Mater. Chem. B*, 2018, **6**, 4274–4292.

29 J. Sahoo and M. De, Gram-selective antibacterial activity of mixed-charge 2D-MoS 2, *J. Mater. Chem. B*, 2022, **10**, 4588–4594.

30 A. Kuroki, J. Tay, G. H. Lee and Y. Y. Yang, Broad-Spectrum antiviral peptides and polymers, *Adv. Healthcare Mater.*, 2021, **10**, 2101113.

31 M. Zare, V. Thomas and S. Ramakrishna, Nanoscience and quantum science-led biocidal and antiviral strategies, *J. Mater. Chem. B*, 2021, **9**, 7328–7346.

32 C. P. Sharma and C. J. Arnusch, Laser-induced graphene composite adhesive tape with electro-photo-thermal heating and antimicrobial capabilities, *Carbon*, 2022, **196**, 102–109.

33 S. Beikzadeh, *et al.*, Charged laser-induced graphene electrodes exhibit strong capacitance-based antibacterial and antiviral properties, *Appl. Mater. Today*, 2023, **31**, 101753.

34 S. P. Singh, Y. Li, J. Zhang, J. M. Tour and C. J. Arnusch, Sulfur-doped laser-induced porous graphene derived from polysulfone-class polymers and membranes, *ACS Nano*, 2018, **12**, 289–297.

35 A. Gupta, *et al.*, Low-Voltage Bacterial and Viral Killing Using Laser-Induced Graphene-Coated Non-woven Air Filters, *ACS Appl. Mater. Interfaces*, 2021, **13**, 59373–59380.

36 G. Wang, *et al.*, An antibacterial platform based on capacitive carbon-doped TiO 2 nanotubes after direct or alternating current charging, *Nat. Commun.*, 2018, **9**, 2055.

37 C. Li, *et al.*, Co_3O_4 Nanowires Capable of Discharging Low Voltage Electricity Showing Potent Antibacterial Activity for Treatment of Bacterial Skin Infection, *Adv. Healthcare Mater.*, 2022, **11**, 2102044.

38 J. Banerjee, *et al.*, Silver-zinc redox-coupled electroceutical wound dressing disrupts bacterial biofilm, *PLoS One*, 2015, **10**, e0119531.

39 J. Tian, *et al.*, A self-powered sterilization system with both instant and sustainable anti-bacterial ability, *Nano Energy*, 2017, **36**, 241–249.

40 T. Cheng, *et al.*, Flexible transparent bifunctional capacitive sensors with superior areal capacitance and sensing capability based on PEDOT: PSS/MXene/Ag grid hybrid electrodes, *Adv. Funct. Mater.*, 2023, **33**, 2210997.

This journal is © The Royal Society of Chemistry 2023

J. Mater. Chem. B, 2023, **11**, 8170–8181 | **8179**

41 T. Cheng, *et al.*, Stretchable and Self-Healing Interlocking All-in-One Supercapacitors Based on Multiple Cross-Linked Hydrogel Electrolytes, *Adv. Mater. Interfaces*, 2022, **9**, 2201137.

42 L. Xiao, *et al.*, Layer-by-layer assembled free-standing and flexible nanocellulose/porous Co_3O_4 polyhedron hybrid film as supercapacitor electrodes, *Adv. Compos. Hybrid Mater.*, 2021, **4**, 306–316.

43 Z. Yang, *et al.*, Double-safety flexible supercapacitor basing on zwitterionic hydrogel: over-heat alarm and flame-retardant electrolyte, *Adv. Compos. Hybrid Mater.*, 2022, **5**, 1876–1887.

44 Y. Wang, *et al.*, Flexible barium titanate@ polydopamine/polyvinylidene fluoride/polymethyl methacrylate nanocomposite films with high performance energy storage, *Adv. Compos. Hybrid Mater.*, 2022, **5**, 2106–2115.

45 T. Cheng, *et al.*, 3D printable conductive polymer hydrogels with ultra-high conductivity and superior stretchability for free-standing elastic all-gel supercapacitors, *Chem. Eng. J.*, 2022, **450**, 138311.

46 C. Lai, *et al.*, High-performance double "ion-buffering reservoirs" of asymmetric supercapacitors enabled by battery-type hierarchical porous sandwich-like Co_3O_4 and 3D graphene aerogels, *Adv. Compos. Hybrid Mater.*, 2022, **5**, 2557–2574.

47 X. Liu, *et al.*, Porous organic polymers for high-performance supercapacitors, *Chem. Soc. Rev.*, 2022, **51**, 3181–3225.

48 A. Ahmed, I. Hassan and C. Ling, Multifaceted, printable skin-integrated electronics for monitoring physiological functions, *J. Mater. Chem. C*, 2022, **10**, 1479–1487.

49 R. Vicentini, *et al.*, Ragone plots for electrochemical double-layer capacitors, *Batteries Supercaps*, 2021, **4**, 1291–1303.

50 Z. Jis, *2801: 2010 Antimicrobial Products-Test for Antimicrobial Activity and Efficacy*, Japanese Standards Association, Akasaka, Minato-ku, Japan, 2010.

51 J. D. Heming, J. F. Conway and F. L. Homa, Herpesvirus capsid assembly and DNA packaging, *Cell Biol. Herpes Viruses*, 2017, 119–142.

52 M. Matrosovich, T. Matrosovich, W. Garten and H.-D. Klenk, New low-viscosity overlay medium for viral plaque assays, *Virol. J.*, 2006, **3**, 1–7.

53 C. E. Garvey, C. L. McGowin and T. P. Foster, Development and evaluation of SYBR Green-I based quantitative PCR assays for herpes simplex virus type 1 whole transcriptome analysis, *J. Virol. Methods*, 2014, **201**, 101–111.

54 H. M. Yadav, *et al.*, Nickel-Graphene nanoplatelet deposited on carbon fiber as binder-free electrode for electrochemical supercapacitor application, *Polymers*, 2020, **12**, 1666.

55 J.-S. M. Lee, M. E. Briggs, C.-C. Hu and A. I. Cooper, Controlling electric double-layer capacitance and pseudocapacitance in heteroatom-doped carbons derived from hypercrosslinked microporous polymers, *Nano Energy*, 2018, **46**, 277–289.

56 X. Liu, *et al.*, Carbon cloth as an advanced electrode material for supercapacitors: progress and challenges, *J. Mater. Chem. A*, 2020, **8**, 17938–17950.

57 T. Zhang, *et al.*, Making a commercial carbon fiber cloth having comparable capacitances to carbon nanotubes and graphene in supercapacitors through a "top-down" approach, *Nanoscale*, 2015, **7**, 3285–3291.

58 Z. Miao, *et al.*, High-performance symmetric supercapacitor constructed using carbon cloth boosted by engineering oxygen-containing functional groups, *ACS Appl. Mater. Interfaces*, 2019, **11**, 18044–18050.

59 Z. Sun, *et al.*, Self-template biomass-derived nitrogen and oxygen co-doped porous carbon for symmetrical supercapacitor and dye adsorption, *Adv. Compos. Hybrid Mater.*, 2021, **4**, 1413–1424.

60 P. Sundriyal and S. Bhattacharya, Textile-based supercapacitors for flexible and wearable electronic applications, *Sci. Rep.*, 2020, **10**, 1–15.

61 J. Huang, *et al.*, Carbon fabric-based self-powered magneto-electric tactile sensors for soft robot's sensing with resistance to acidic/alkaline environments, *J. Mater. Chem. C*, 2021, **9**, 14827–14837.

62 X. Zhang and J. Dutta, X-Fe (X= Mn, Co, Cu) Prussian Blue Analogue-Modified Carbon Cloth Electrodes for Capacitive Deionization, *ACS Appl. Energy Mater.*, 2021, **4**, 8275–8284.

63 M. Gineys, R. Benoit, N. Cohaut, F. Béguin and S. Delpeux-Ouldriane, Behavior of activated carbon cloths used as electrode in electrochemical processes, *Chem. Eng. J.*, 2017, **310**, 1–12.

64 D. Ye, Y. Yu, J. Tang, L. Liu and Y. Wu, Electrochemical activation of carbon cloth in aqueous inorganic salt solution for superior capacitive performance, *Nanoscale*, 2016, **8**, 10406–10414.

65 Q. Hu, *et al.*, Superhydrophilic phytic-acid-doped conductive hydrogels as metal-free and binder-free electrocatalysts for efficient water oxidation, *Angew. Chem.*, 2019, **131**, 4362–4366.

66 Z. Yao, B. Quan, T. Yang, J. Li and C. Gu, Flexible supercapacitors based on vertical graphene/carbon fabric with high rate performance, *Appl. Surf. Sci.*, 2023, **610**, 155535.

67 S. Arshadi Rastabi, *et al.*, Treatment of NiMoO4/nanographite nanocomposite electrodes using flexible graphite substrate for aqueous hybrid supercapacitors, *PLoS One*, 2021, **16**, e0254023.

68 D. K. Maurya, R. Dhanusuraman, Z. Guo and S. Angaiah, Composite polymer electrolytes: progress, challenges, and future outlook for sodium-ion batteries, *Adv. Compos. Hybrid Mater.*, 2022, **5**, 2651–2674.

69 Y. Fang, *et al.*, Phosphorus and sulfur codoped carbon nitride nanosheets with enhanced photocatalytic antibacterial activity and promotion of wound healing, *Appl. Surf. Sci.*, 2022, **586**, 152761.

70 S. Z. Scalinci and E. T. Battagliola, Conjunctivitis can be the only presenting sign and symptom of COVID-19, *IDCases*, 2020, **20**, e00774.

71 D. Eke, *et al.*, Apoptotic gene expression profiles and DNA damage levels in rat liver treated with perfluorooctane sulfonate and protective role of curcumin, *Int. J. Biol. Macromol.*, 2017, **104**, 515–520.

72 H.-y Zhou, *et al.*, Anti-HSV-1 effect of dihydromyricetin from Ampelopsis grossedentata via the TLR9-dependent anti-inflammatory pathway, *J. Global Antimicrob. Resist.*, 2020, **23**, 370–376.

73 P. D. Rakowska, *et al.*, Antiviral surfaces and coatings and their mechanisms of action, *Commun. Mater.*, 2021, **2**, 1–19.

74 Y. Wang, *et al.*, Cationic phenylene ethynylene polymers and oligomers exhibit efficient antiviral activity, *ACS Appl. Mater. Interfaces*, 2011, **3**, 2209–2214.

75 I. S. Donskyi, *et al.*, Functionalized nanographene sheets with high antiviral activity through synergistic electrostatic and hydrophobic interactions, *Nanoscale*, 2019, **11**, 15804–15809.

This journal is © The Royal Society of Chemistry 2023

J. Mater. Chem. B, 2023, **11**, 8170–8181 | **8181**